Advances in Science and Technology Research Journal

Advances in Science and Technology Research Journal, 2026, 20(9), 424–436
https://doi.org/10.12913/22998624/224953
ISSN 2299-8624, License CC-BY 4.0

Received: 2026.02.11
Accepted: 2026.07.10
Published: 2026.08.01

Effect of tool geometry and welding parameters on shear strength and microstructural characteristics of AA6061-T6/PMMA friction stir lap joints

Lingerew Enbakom Melaku[1*], Jacek Tomków[1]

[1] Faculty of Mechanical Engineering and Ship Technology, Gdańsk University of Technology, ul. Gabriela Narutowicza 11/12, 80-233 Gdańsk, Poland
* Corresponding author's e-mail: lingerew.melaku@pg.edu.pl

ABSTRACT

Dissimilar joints between aluminum and polymer have gained significant interest in the transportation, aerospace, and marine industries due to their potential for lightweight applications. In the present study, the joint performance analysis of dissimilar material joints of AA6061-T6 aluminum alloy and poly(methyl methacrylate) (PMMA) was performed utilizing friction stir welding (FSW) in the lap joint. Shear strength testing and optical microscopy were employed to evaluate joint performance and defect formation. Joints produced using a concave shoulder tool exhibited lower thermal degradation of PMMA and improved surface quality than a flat shoulder tool. The macro- and microstructural analyses revealed joint defects such as cracks, tunnels, voids, and uneven distribution of AA6061-T6 and PMMA particles. Analysis of variance (ANOVA) revealed that rotational speed was the most influential parameter (41.16%), followed by tool geometry (34.43%) and welding speed (14.69%). The maximum shear strength of 17.8 MPa was obtained at 925 rpm and 60 mm/min using a tapered pin with a flat shoulder.

Keywords: shoulder profile, lap joint, shear strength, microstructural analysis, pore size.

INTRODUCTION

Thermoplastic polymers are increasingly replacing metals in industries such as aerospace, marine, and automotive to achieve thermal and electrical insulation, design flexibility, weight reduction of the structure, and corrosion resistance [1]. Due to this broad range of applications, high-quality joints are required. Research on joining dissimilar aluminum alloys to thermoplastic polymers aims to exploit the combined properties of both materials. Aluminum alloy AA6061-T6 and poly(methyl methacrylate) (PMMA) are frequently used for automobile sheet panels due to their high corrosion resistance properties. Among various polymers, PMMA is a thermoplastic that is widely used in the automotive industry as a substitute for glass or the expensive plastic parts due to its prominent thermal and chemical stability [2]. PMMA is an economical alternative to replace polycarbonate (PC) when strength and transparency are more important than impact strength, chemical resistance, and heat resistance [3]. Therefore, the hybrid aluminum/polymer structures have great potential applications for these industries [4]. However, the significant difference in thermal conductivity, and chemical properties between metal and polymer makes the welding process a challenging task. The remarkable complexity of Al/polymer joining methods has driven extensive investigations aimed at identifying the most effective approaches for achieving defect-free joints.

The heat input in FSW increases with rotational speed and decreases with welding speed, directly affecting the resulting microstructure and mechanical properties [5]. Several studies have investigated the effect of process parameters such as rotational speed, welding speed, tilt angle, and plunge depth on material flow pattern, microstructure, and surface morphology. Derazkola et al [4] investigated the effect of tilt angle and plunge depth using a concave shoulder and tapered pin welding tool on tensile strength of aluminum alloy AA5058/PMMA lap joint at a constant rotational and welding speed. The author reported that the highest strength of 45 MPa, 60% of polymer strength, was attained at optimum process parameters. Later, Derazkola and Simchib [3] improved the joint efficiency up to 50 MPa, 71% of the polymer strength, through the optimization of rotational speed, welding speed, tilt angle and plunge depth for AA5754/PMMA T-joint. Derazkola and Simchib [6] further improved the tensile strength up to 61 MPa suing in-situ nanoparticles injection methods with the same optimum parameters from their previous publication. Although these studies performed a progressive improvement of joint performance, the effect of material, aluminum alloys (AA5058, AA5754, and AA6062), and joint configurations (lap and T-joints) were not explicitly mentioned.

Dalwadi et al [7] studied the effect of rotational speed and welding speed on tensile strength of AA6061/PMMA FSW joints with a constant plunge depth of 2.8 mm and tool tilt angle of 2°. The highest tensile strength of 7.076 MPa was recorded at a rotational speed of 1000 rpm and a welding speed of 40 mm/min, where better mechanical interlocking was observed. Studies showed that rotational speed is most influential parameter in FSW, followed by tool geometry and the welding speed [8, 9]. However, several studies also explained the influence of process parameters depend on the material properties. For example, welding speed was appeared as a dominant factor in FSW AA2198-AA6082 [10], and aluminum/GFRP joint [11] and plunge depth was a highest influence in AA6082-T6/PA6 joints [12]. According to the review conducted by Kasgari et al [13], defects such as excessive flash, tunnel defects, porosity, and incomplete penetration are common in metal/polymer FSW joints. Numerous studies have been published on FSW of metal/polymers in literature and determined the influences of process parameters on joint quality, some of the reported are given in Table 1. Previous studies have shown that optimization of welding parameters to reduce joint defects; however, controlling heat generation remains major challenges in metal/polymer FSW.

Along with the process parameters optimization, some studies applied additional improvement such as preheating [14], injection of Al_2O_3 nanoparticles [15], adding a surface texture using a laser ablation [16, 17], and surface treatments such as sandblasting, anodizing, or plasma activation [18, 19]. These modifications aim to promote uniform distribution between metal and polymer particles, improve mechanical interlocking and the overall joint performance. However, joint defects such as voids, polymer overflow, and bubble formation were observed. For example, excessive preheating reduce the material flow quality and increase defects. Although few modified techniques have been proposed, the fundamental influence of basic welding parameters still required further investigation.

From the literature review, it is evident that a moderate number of experimental studies have investigated FSW aluminum/polymer joints, focusing primarily on the influence of process parameters such as rotational speed, welding speed, tilt angle, plunge depth and tool geometry on the joint performance. However, limited studies have specifically addressed the influence of tool geometry on thermal degradation and surface quality of polymer during dissimilar FSW of metal/polymer. To the best of the authors' knowledge, the influence of tool geometry on polymer thermal degradation and surface quality during FSW of aluminum/polymer has received limited attention in the literature. In this study, an effort was made to improve surface quality without compromising shear strength of FSW AA6061-T6/PMMA hybrid lap joints. The present study aims to show the effect of tool geometry, rotational speed and welding speed on joint surface quality, shear strength and microstructural characteristics. The results showed a significant improvement in surface quality of the top plate (PMMA) with reduced pyrolysis and thermal damage when using a concave shoulder. Unlike most published studies conducted on material thicknesses of 4 mm or less, this study utilizes a material thickness of 5 mm.

MATERIALS AND METHODS

In this study, AA6061-T6 aluminum alloy and PMMA plates of 5 mm thickness were used as the base materials. The base material plates were cut to the dimensions of 150 × 60 × 5 mm using an automatic hacksaw. Appropriate clamping was employed to prevent slippage of the top material

Table 1. Effects of process parameters on weld responses in FSW of dissimilar aluminum alloy with polymers

Metal-polymer	Joint configuration	Welding parameters	Joint characterization	Conclusion	Joint defects	Reference
AA6082-T6 – glass fiber-reinforced (GFR) polyphenylene ether (PPE)	Lap joint	Tilt angle, welding speed, rotational speed	Tensile strength, morphology	Joint efficiencies between 10.1 and 47.4%	Cracks, voids and gaps	[20]
Al6061- glass fiber–reinforced thermoset polymer (GFRP)	Lap joint	Welding speed, plunge depth, rotational speed	Microstructure, shear strength, chemical bond formation	94% in joint strength		[11]
AA6082-T6-Noryl GFN2 polymer	Buttstrap configuration	Rotational speed, welding speed	Tensile, flexural behavior, microstructural	tensile efficiency 27.7-47.9% referred to AA6082-T6		[21]
AA5052-H32/PC	Lap joint	Tool geometry	Microstructural analysis, shear strength			[22]
AA1050 -polyether-ether-ketone (PEEK)	Fastenerless-friction stir extrusion~lap spot	Rotation, linear movement, plunge depth, tilt angle	Visual inspection	Friction stir forming, strong joint using GFRP	Melting of PEEK surface, PEEK thermal softening	[23]
6061-T6/ carbon fiber reinforced thermoplastic (CFRTP)	Lap joint	Rotational speed,	Microstructure, fracture, tensile strength, hardness	Clean surfaces, distributed Al fragments, 63.1% tensile of base CFRTP's strength	Tunnel defects, carbonized polymer	[24]
AA5052 -(CF/ PEEK)	Lap joint	Rotational speed, surface conditions (Sandblasting, Mechanical Engraving	tensile shear force and joint morphology	6.7 MPa joint strength	Voids, surface crack, PEEK squeeze-out	[25]
AA5754/PEEK	Lap joint	Tool geometry, lateral offset	Tensile shear, microstructure, SEM analysis	Shear strength of 110 kN/m, consolidated aluminum ceiling	Voids / Porosity, weak interlock,	[26]
AA7075/ low-density polyethylene (LDPE)	Butt joint	Welding speed, rotational speed, silicon carbide (SiC) nanoparticles	Microhardness, tensile strength, bending test	SiC reduce melt instability, Joint efficiency reaches ~70%,	Shrinkage voids, porosity, clustering of nanoparticle	[27]

over the aluminum alloy plate. The mechanical and thermal properties of base materials and chemical composition of AA6061-T6 are presented in Table 2 and Table 3, respectively. The welding was conducted on a 3-axis universal milling machine as shown in Figure 1a along the 150 mm length. The aluminum alloy and PMMA plates were joined using FSW in a lap joint configuration, with the PMMA positioned on top, Figure 1b.

The tool rotational speed of (680 rpm, 925 rpm, 1235 rpm, and 1750 rpm), welding speed (30 mm/min, 60 mm/min), and tool geometry were used as varying process parameters. A constant plunge depth of 0.2 mm was employed for all sets of experiments. The welding tools were machined from NC6 tool steel and hardening heat treatment was applied. Four distinct tool geometries were employed, as illustrated in Figure 2; namely, a flat shoulder with a cylindrical pin, a flat shoulder with a tapered pin, a concave shoulder with a cylindrical pin, and a concave shoulder with a tapered pin. The dimensions of shoulder diameter, pin diameter, pin length, taper angle and concavity angle of the tools are shown in Figure 2. For example, the tool feature of a 22 mm- shoulder diameter with a 7° concave angle and tapered pin profile with a pin length of 6 mm. The tapered pin has a larger diameter of 7 mm and a smaller diameter of 3 mm. The concave shoulder enhances material consolidation and reduces outward flow by improving material mixing. A large shoulder diameter with a concave feature and a shorter tapered pin enhances the material flow and improve the joint strength [28].

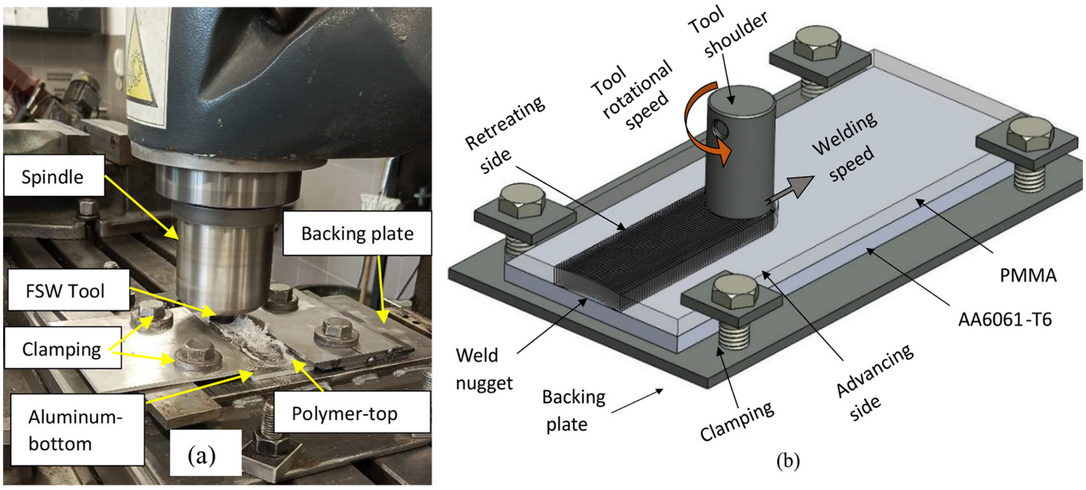

Figure 1. Clamping fixtures: a) FSW experimental setup, b) schematic illustration of AA6061-T6 and PMMA FSW process

A mixed-level fractional factorial design was adopted to reduce the number of experiments from the full factorial design (4 × 4 × 2 = 32 runs) to 16 runs, followed by two confirmation experiments. The confirmation experiments were selected based on the best-performing condition from visual inspections. The effect of shoulder profile, pin profile, rotational speed, and welding speed were then investigated.

According to several studies, heat generation in FSW is primarily governed by tool rotational speed, and tool geometry followed by welding speed [4, 29]. Optimizing these two parameters can therefore enhance joint quality. Finding the optimum rotational speed sufficient to plasticize aluminum and not to thermally degrade the PMMA, is always a meaningful and challenging task in this dissimilar FSW. The soundness of dissimilar joint was primarily influenced by the key processing parameters in terms of the rotational and welding speed of the tool [30].

Table 2. Mechanical and thermal properties of AA6061-T6 aluminum alloy and PMMA [7]

Base materials	AA6061	PMMA
Glass transition temperature(Tg) (°C)		106
Density (kg/m3)	2.7	1190
Thermal conductivity (W/m K)	167	0.2
Ultimate tensile strength (MPa)	318	77
Elongation (%)	11	6
Hardness	95BHN	90 ShoreD
Shear strength (MPa)	207	140
Melting Point (°C)	582-652	
Thermal degradation (°C)		160

RESULTS AND DISCUSSION

The following sections discuss the mechanical performance of nine selected joints: three high-strength (W4, W5, and W11), three intermediate-strength (W1, W12, and W16), and three low-strength (W6, W13, and W17) joints. These joints were selected based on their shear strength results (Table 4) and are used to establish correlations between process parameters, microstructural characteristics, and failure behavior.

Visual inspection

The effect of shoulder profile on the weld surface morphology of the joints was investigated using flat and concave shoulder tools. Blackened regions indicate localized thermal degradation of PMMA due to excessive heat input at the heat affected zone (HAZ), thermo-mechanical affected zone (TMAZ) and stir zone (SZ). In contrast, whitish-translucent appearance was also achieved. The shoulder profile was the main factor for the surface clarity or irregularities of the joint. In spite of rotational speed, welding speed, and pin profile, the degradation and discoloration of PMMA was mostly related to the shoulder profile. Although shear strength is comparable for both shoulder profiles, concave shoulder gave a great advantage to minimize the thermal degradation. The aesthetics and absence of visible thermal

Table 3. Chemical composition of AA6061-T6 (wt.%)[7]

Al	Mg	Si	Fe	Cu	Cr	Mn	Ti	Zn	Others
Balance	1.05	0.63	0.29	0.27	0.17	0.07	0.02	0.01	<0.1

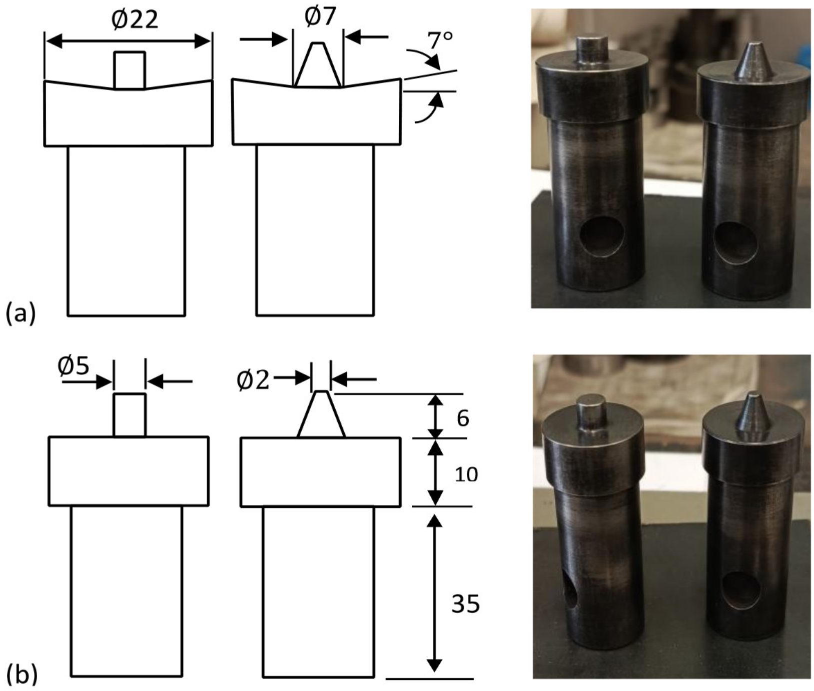

Figure 2. FSW tool geometries; tool dimensions, CAD design and fabricated tools. (a) A concave shoulder with a cylindrical pin and a concave shoulder with a tapered pin, (b) A a flat shoulder with a cylindrical pin, a flat shoulder with a tapered pin

Table 4. Design of experiments based on based fractional factorial design and response output

Joint ID	Rotational Speed (rpm)	Welding speed (mm/min)	Shoulder profile	Pin profile	Load (Kgf)	Shear strength (MPa)
W1	680	30	Flat shoulder	Cylindrical	460	15.6
W2	680	60		Tapered	305	11
W3	925	30		Cylindrical	220	9.7
W4	925	60		Tapered	510	17.8
W5	1235	30		Cylindrical	472	16.2
W6	1235	60		Tapered	146	4.6
W7	1750	30		Cylindrical	217	9.5
W8	1750	60		Tapered	299	10
W9	925	60		Tapered	504	17.6
W10	680	30	Concave shoulder	cylindrical	347	13.1
W11	680	60		Tapered	497	17.5
W12	925	30		cylindrical	273	11.7
W13	925	60		Tapered	311	10.7
W14	1235	30		cylindrical	210	9.5
W15	1235	60		Tapered	316	11
W16	1750	30		cylindrical	324	12.8
W17	1750	60		Tapered	309	9.2
W18	680	30		Tapered	521	17.4

damage by the concave shoulder is a critical processing advantage, particularly for applications where surface quality, cosmetic appearances are prioritized. The difference in surface morphology from visual inspection provides the first indication of heat input stability and provides guidance to the subsequent cross-sectional and microstructural analyses. The weld surface using flat shoulder shown in Figure 3a, which is thermally damaged and blacken also observed by Derazkola et al [4]. The photograph of four joints using flat and concave shoulder are shown in Figure 3a and b with similar process parameters but different shoulder profiles associated with weld joints W4, W5, W11 and W12 from Table 4.

Microstructural analysis

The samples were sectioned perpendicular to the joint line, ground using progressively finer SiC abrasive papers and polished. The microstructure image of the joint was examined using optical microscopy at SZ, and the micrographs of selected joints are given in Figure 4. The microstructural analysis reveals that the uneven stirring of the materials at the interface results in defects such as cracks, bubbles, voids, and tunnel defects were observed. The optimum tool design, welding speed and rotational speed influence the joint microstructure, grain refinement in aluminum and interfacial morphology evolution as reported by Shinde and Arakerimath [31]. The microstructure features and distribution of Al and PMMA across the joint related to the lap shear strength.

The materials interlock between the joint materials; aluminum alloy particles embedded into PMMA was observed. Improved material mixing observed in Figure 4b correlates with higher shear strength (joint ID, W5), indicating that better mechanical interlocking obtained in these process parameters. The mechanical interlocking mechanisms and physical adhesion at the interface, which significantly influence joint strength and durability. The observed microstructural related to the joint performance, particularly the extent of material intermixing and defect formation. The details of material deformation, grain refinement, and phase distribution across the weld interface, providing insights into optimizing process parameters for enhanced joint integrity. Furthermore, the extent of plastic deformation and material flow, identifying regions of high strain and potential defect formation, such as voids or tunnels that could compromise the joint's performance [32].

The optical micrograph images shown in Figure 4 represent joints with high, moderate, and low performance. The joints having higher shear strength show a better material intermixing as shown in Figure 4 (a-c). The aluminum particles embedded into PMMA and vice versa. The joint defects significantly lower than other joints except uneven distribution of metal and polymer particles and small voids.

Joint W4, fabricated with a flat shoulder, tapered pin, rotational speed of 925 rpm, and welding speed of 60 mm/min, exhibits the most homogenous material flow at SZ with a noticeable aluminum alloy stirring into polymer as shown in Figure 4a.

The pore size distribution histograms presented in Figure 5 provide quantitative insight

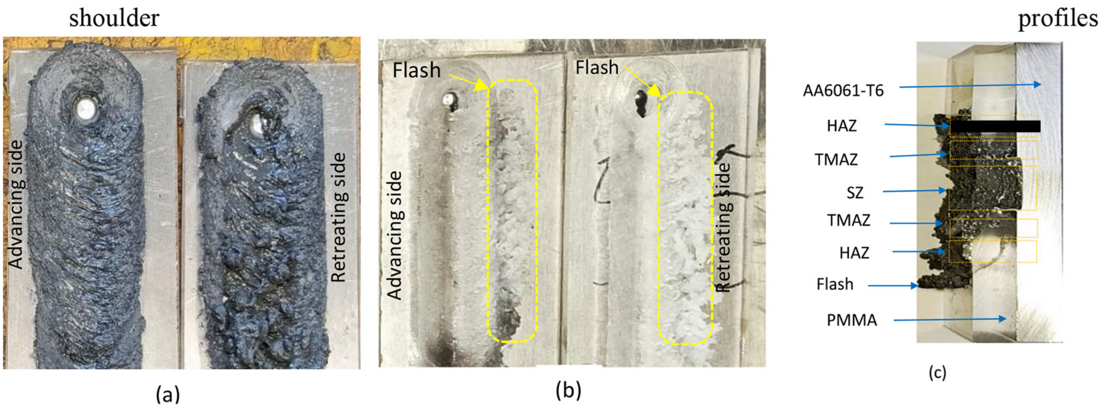

Figure 3. Surface material flow appearance of welded joints produced using different shoulder profile: (a) using flat shoulder (W4 and W5), (b) using concave shoulder (W11 and W12), (c) cross-sectional view indicating joint zones

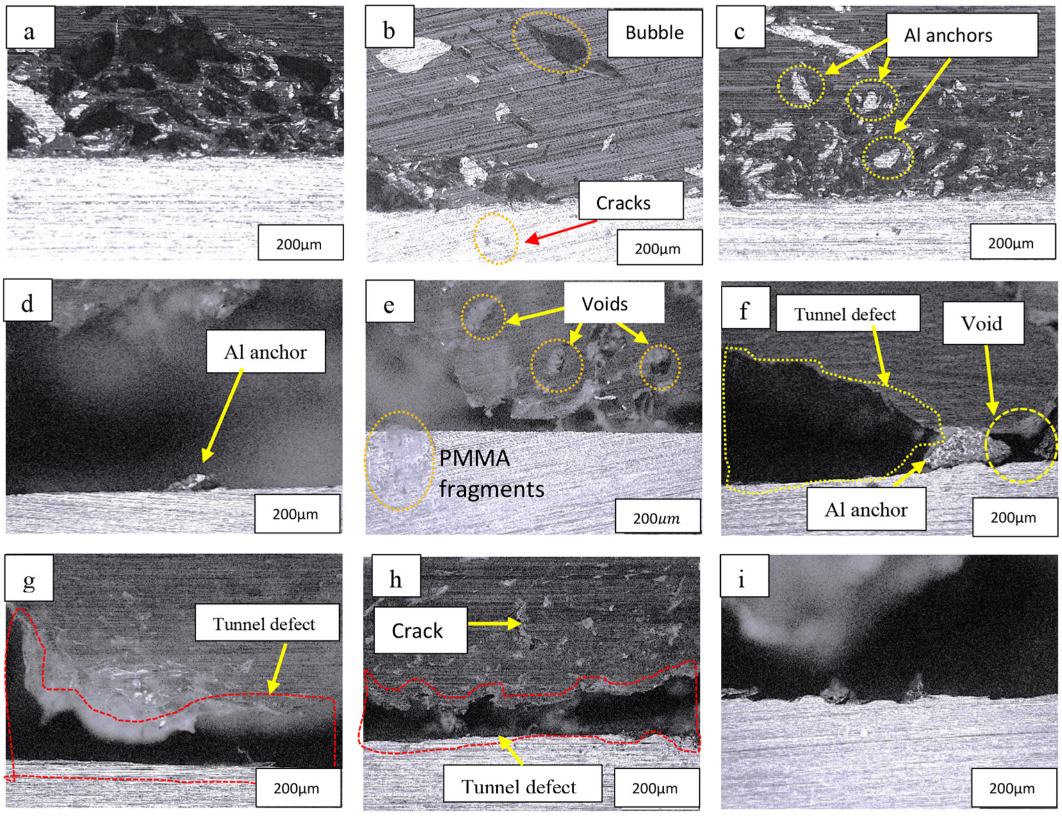

Figure 4. Optical micrographs joints: (a-c) small voids but better material interlock at the interface (W4, W5, and W11), (d-f) bubble, interfacial cracks and aluminum anchors (W1, W12, and W16), and (g-i) tunnel defect indicating limited material mixing (W6, W13, and W17)

into defect formation within the SZ of the dissimilar AA6061-T6/PMMA joint. Asymmetry in pore size characteristics was observed between the polymer and aluminum sides, reflecting the fundamental difference in deformation and thermal responses of the two materials during FSW. From PMMA side, Figure 5a, the pore size distribution exhibits a broad range, with a dominant peak at small pore sizes (~5 µm) and a significant tail extending up to ~15 µm. This wide distribution indicates the coexistence of multiple defect formation mechanisms. Primarily, thermal degradation of PMMA at elevated temperature lead to gas evolution, which become entrapped within the viscous polymer matrix during cooling, forming bubbles and shrinkage voids. In addition, insufficient consolidation and unstable material flow near the interface contribute to the formation of larger voids. The presence of such heterogeneous porosity is indicative of localized overheating and poor control of heat input. Although temperature was not directly measured, heat input trends were inferred from process parameters and observed microstructural features. In contrast, the aluminum side, Figure 5b, exhibits a narrow pore size distribution, predominantly within the range of 1–2 µm. This stable plastic deformation of AA6061-T6 under solid-state conditions, where defect formation is mainly associated with minor flow instabilities rather than gas entrapment. The absence of large pores suggests effective material consolidation and more uniform stirring within the metallic region.

The observed asymmetry in pore distribution attributed to particularly the aluminum and PMMA thermal conductivity and softening behavior. Aluminum, with its high thermal conductivity, dissipates heat efficiently and undergoes controlled plastic deformation, whereas PMMA, with low thermal conductivity and a narrow processing window above its glass transition temperature, is highly susceptible to thermal degradation and bubble formation. Furthermore, the extent of porosity on the PMMA side is expected to have a direct influence on joint performance. Increased pore size and density reduce the effective load-bearing area and weaken the mechanical interlocking at the interface, thereby contributing to lower shear strength. Consequently, minimizing pore formation through optimized heat input,

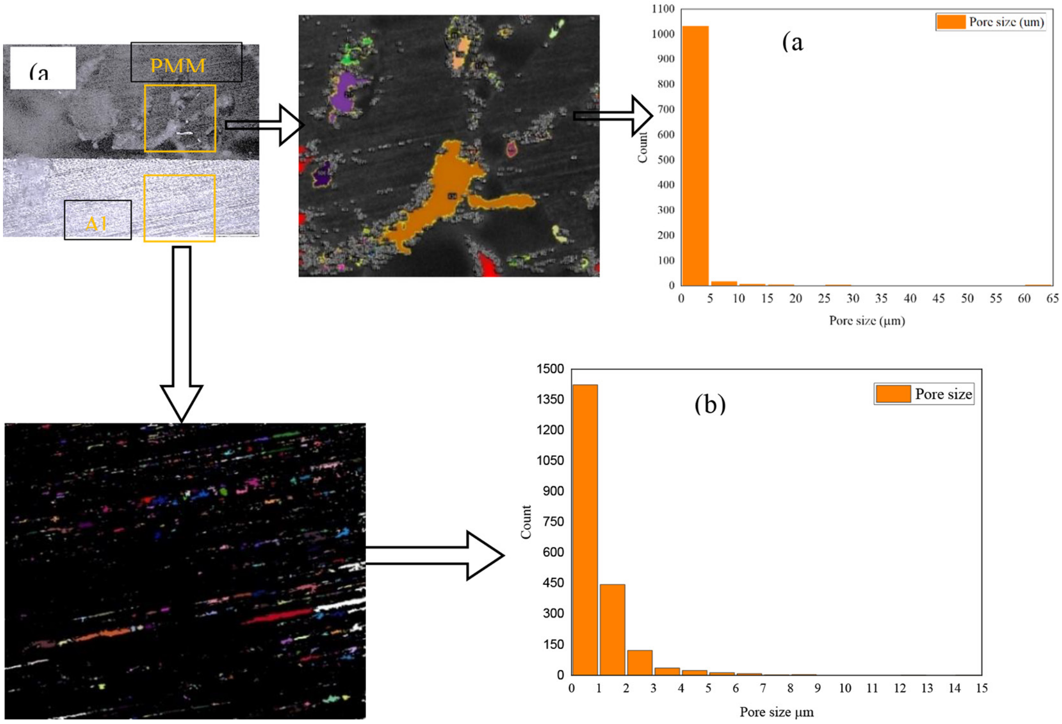

Figure 5. Pore size distribution in the SZ: (a) histogram of pore size distribution on the PMMA sid, (b) pore size distribution on the AA6061-T6 side

achieved by appropriate selection of rotational speed, welding speed, and tool geometry, is critical to improve joint integrity.

To minimize the observed tunnel defects, voids, bubbles, and micro-cracks, enhanced thermal management strategies are recommended, such as the implementation of a stationary shoulder or localized cooling systems immediately trailing the tool. These methods would effectively regulate the thermal cycle, preventing the PMMA from exceeding its degradation temperature. Furthermore, precise control of the tool plunge depth is critical to maintain plasticized aluminum at the interface.

Shear strength

Shear testing is the most relevant characterization that offers a comprehensive understanding of the weld joint quality by evaluating how well the two materials are bonded together. Shear strength is a key metric for evaluating joint performance to measure the ability to withstand forces acting parallel to the weld line [33]. The shear strength of all joints are shown in Table 4 and photographs of the fractured specimens are shown in Figure 6c.

The single-lap shear strength of the joints was measured using a universal testing machine (UTM), shown in Figure 6. The maximum load (Kgf) was recorded from the machine's analog indicator at failure occurrence. Shear strength is calculated by dividing the maximum shear force acting on a material by its cross-sectional area, Equation 1. All specimens' failure mechanism is associated with the Al/PMMA joint interface at the SZ without noticeable plastic deformation. The maximum lap shear strength of 17.8 MPa was recorded under optimal parameters of a rotational speed of 925 rpm and a welding speed of 60 mm/min using a flat shoulder and tapered pin. But, for a concave shoulder, the optimum parameters was a rotational speed of 680 rpm, a welding speed of 30 mm/min, and a cylindrical pin with shear strength of 17.5 MPa. As mentioned in section 2, the confirmation experiment was performed at the parameters combination of rotational speed 680 rpm, welding speed 30 mm/min, concave shoulder and tapered pin profile.

$$Shear\ strength(\tau) = \frac{F_{max}}{A_{cross-section}} \quad (1)$$

where: F_{max} – maximum load carrying capacity and $A_{cross-section}$ – shear area.

The maximum shear strength obtained in this study, 17.8 MPa, is comparable to several reported values for similar aluminum/polymer friction stir lap joints. For instance, Dalwadi et al [7] reported a tensile strength of approximately 7 MPa for AA6061/PMMA joints under conventional processing conditions. However, higher strengths in the range of 45–60 MPa have been reported by Derazkola et al. [4] under optimized conditions involving different joint configurations and additional process enhancements. These variations indicate that joint strength is highly dependent on material systems, process optimization, and auxiliary techniques. In this context, the results obtained in the present study fall within the expected range for unmodified AA6061-T6/PMMA lap joints. While the maximum shear strength of 17.8 MPa represents approximately 23% of the base PMMA tensile strength, this joint efficiency is notable considering the significant thickness of 5 mm plates used in this study. Unlike thinner material joining, the increased thermal on AA6061-T6, inherently risks polymer degradation; thus, achieving nearly a quarter of the base material strength provides a viable insights for further process optimization.

The concave shoulder keeps the plasticized material within and promotes material mixing at the interface. A flat shoulder, on the other hand, forces the softened material out of the stir zone, which causes excessive flash and thermal degradation defects. A high shoulder diameter with a concave feature and a short, tapered pin improves the material flow through the weld joint, which makes the joint stronger [34]. The concavity of the shoulder accommodates the volume of heated material, increases material flow, and directs the deformed material from the edge of the shoulder to the pin. The concave shoulder helps to maintain the deformed material in the stir zone (SZ) by preserving it within the concave region and allowing the tool to feed it back into the weld area [35]. Higher rotational speeds lead to excessive softening and thermal degradation of PMMA beyond its glass transition temperature. And lower rotational speed generates insufficient heat to plasticize aluminum, so the two materials are not stirred properly. Welding speed and dwelling time are also other parameters that contribute to the quality of the joint. The lowest shear strength was observed at the higher rotational speed and welding speed as shown in Figure 7(a) for both concave and flat shoulder tool geometry. For example, joint W8 at rotational speed of 1750 rpm, welding speed 60 mm/min, flat shoulder and tapered pin profile was less than average shear strength and the

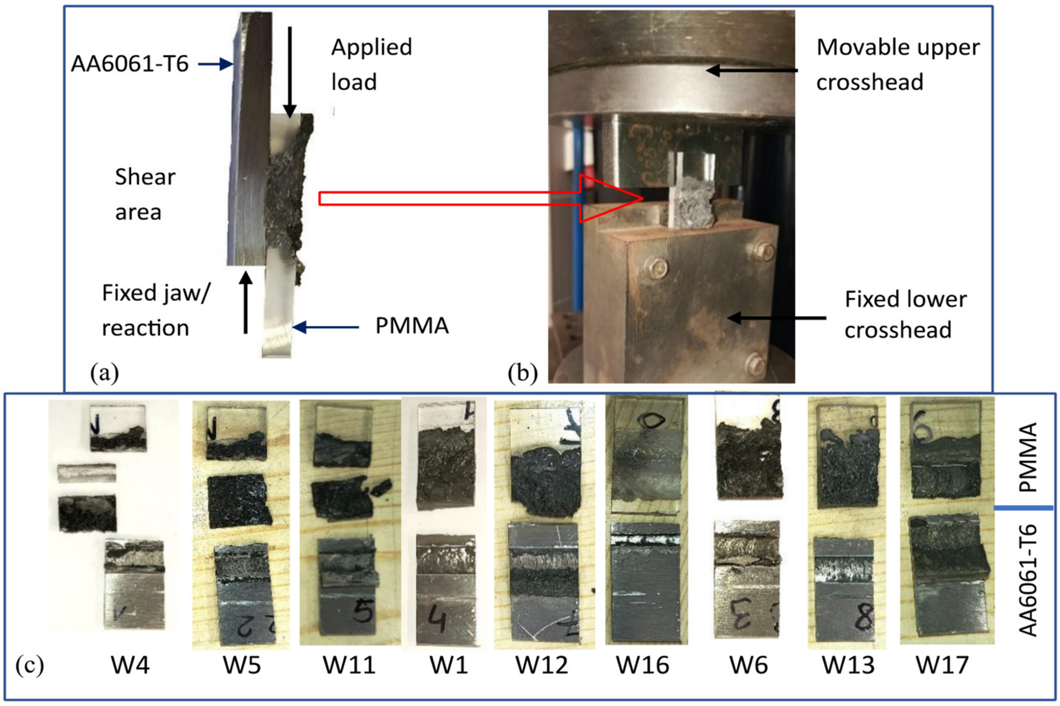

Figure 6. Lap shear testing of FSW joints: (a) prepared sample for shear testing, (b) experimental setup in the universal testing machine, (c) fractured specimens of selected joints

joint was failed in interfacial debonding failure mechanism, Figure 6b. This failure mechanism is the indication of kissing bond defect unlike the partial interfacial fracture.

The contour plot in Figure 7a, show the influence of rotational and welding speeds on shear strength. The graphic illustrates that achieving a sound weld necessarily either the combination of lower rotational speeds (~800–1100 rpm) and higher welding speeds (~50–60 mm/min) or higher rotational speeds (~1400–1600 rpm) and lower welding speeds (~30–45 mm/min). This interaction indicates that heat input and material flow must be balanced to achieve sufficient aluminum plasticization while avoiding excessive polymer degradation. When the rotational and welding speeds are higher at a time, it produce substantial heat and turbulent flow, resulting in reduced shear strengths and macroscopic defects such as tunneling or surface cracks, Figure 4(g-i). Conversely, the combination of lower rotating speeds and lower welding speed yields insufficient heat input to plasticize AA6061-T6. This interaction map provides a solid basis for identifying optimal processing windows that balance enough softening with suitable stirring to a lesser defect joint.

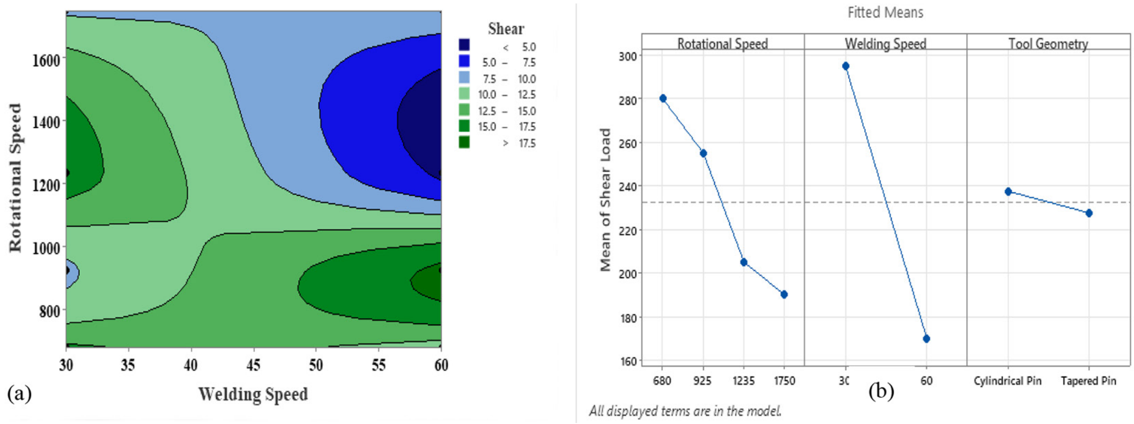

Figure 7. Effect of process parameters on shear strength: (a) contour plot showing effect of rotational speed and welding speed on shear strength, (b) main effects plot

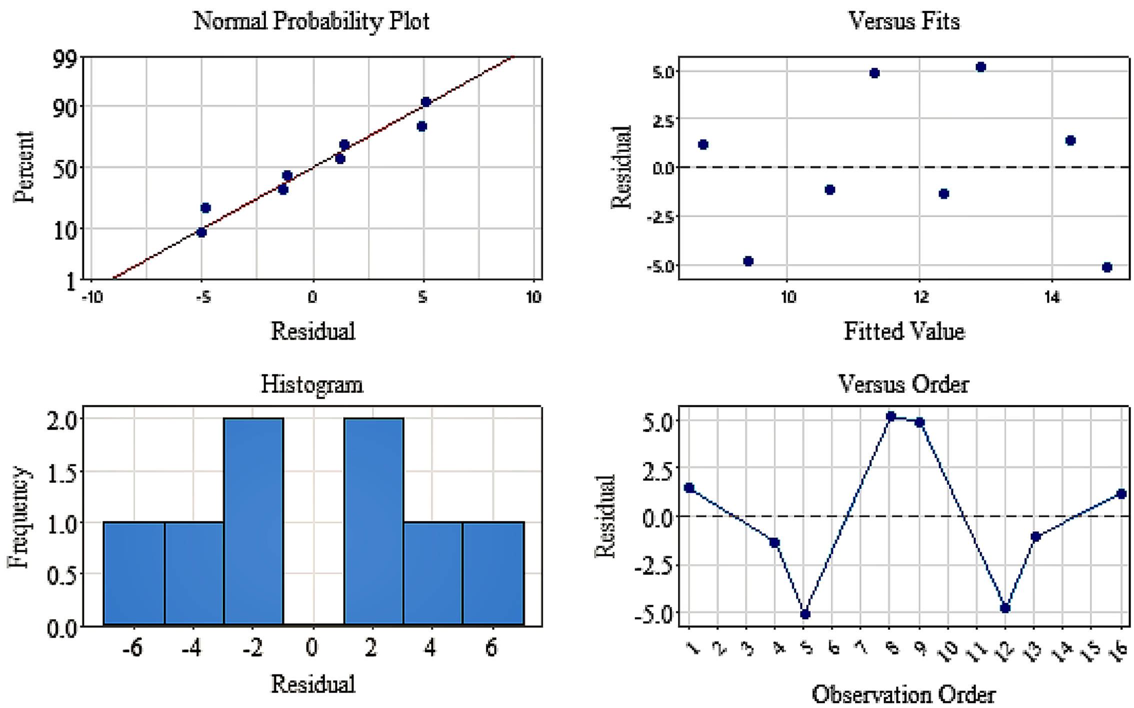

Figure 8. Main effect plots and residual plots obtained for shear strength

Table 5. ANOVA in general linear model for flat shoulder tool

Source	DF	Sum Sq	Mean Sq	F	P	% Contribution
Rotational speed	3	58.178	19.3927	2.823	0.272	41.16
Welding speed	1	20.769	20.769	3.023	0.224	14.69
Tool geometry	1	48.659	48.6591	7.083	0.117	34.43
Residual	2	13.74	6.8698	---	---	9.72

Table 6. ANOVA in general linear model for concave shoulder

Source	DF	Sum Sq	Mean Sq	F	P	% Contribution
Rotational speed	3	309.314	103.105	20.414	0.069	73.02
Welding speed	1	1.498	1.498	0.297	0.6149	10.45
Tool geometry (pin profile)	1	1.498	1.498	0.297	0.6149	10.45
Residual	4	20.203	5.051	–	–	6.08
Total	9	332.513	–	–	–	100

The statistical method, analysis of variance (ANOVA), showed the percentage influence of all three process parameters on shear strength (Figure 8). According to the ANOVA results shown in Table 5 and 6, rotational speed was the most influential parameter on the shear strength, contributing approximately 41.16% and 73% for flat and concave shoulder, respectively. Tool geometry was the second influential parameter, contributing about 34.43%. The study show the shoulder and pin profile have a significant effect on material flow and bonding at the interface. The third parameter, welding speed, contributes 14.69%, which was the smallest among the three process parameters but still have considerable influence. The residual error was 9.72%, which shows that all the selected process parameters explained most of the changes in shear strength, even though a fractional factorial design has limited degrees of freedom. None of the factors reached statistical significance at the 95% confidence level due to the lower residual degrees of freedom (DF = 2). However, the percentage contributions are a better way to evaluate how important each factor is. This aligns with the established guidelines for unreplicated or minimally replicated DOE studies, wherein p-values can be considered unreliable and effect magnitudes are preferred for engineering decision-making. The percentage contribution analysis indicates that the main factors that affect shear strength in this process are rotational speed and tool geometry. Welding speed has a smaller effect, and experimental noise is still low.

CONCLUSIONS

The present study systematically evaluated the influence of tool geometry and process parameters on shear strength and microstructural characteristics of AA6061-T6/PMMA FSW joints. The following conclusions are drawn:

The maximum shear strength of 17.8 MPa achieved in this study, a joint efficiency of approximately 23% of base PMMA tensile strength (77 MPa). For a 5-mm thickness of the aluminum plates, which increases heat dissipation challenges, this strength level provides a fundamental benchmark for the thick-gauge hybrid FSW.

Tool geometry was identified as a critical determinant of surface integrity and thermal degradation. While shear strengths were comparable between shoulder types, the concave shoulder acted as a physical barrier that circumscribed the softened polymer, effectively suppressing “flash” formation and preventing the localized charring observed with flat-shoulder variants.

The ANOVA results confirmed that rotational speed is the primary process, contributing 41.16% and 73% to joint strength for flat and concave shoulders, respectively. This highlights the extreme sensitivity of PMMA viscosity to frictional heat; precise thermal management is required to balance aluminum plasticization with the prevention of polymer pyrolysis.

Microstructural analysis revealed that high-rotational speed leads to bubble and tunnel defects formation. A stationary shoulders and localized cooling systems is recommended to minimize defects due to higher friction heat.

REFERENCES

1. Kumar D., Ganguly S., Acherjee, B. and Kuar, A. S. Performance evaluation of TWIST welding using machine learning assisted evolutionary algorithms, Arab. J. Sci. Eng., Feb. 2024; 49(2): 2411–2441, https://doi.org/10.1007/s13369-023-08238-1
2. Elyasi M. and Derazkola H. A., Experimental and thermomechanical study on FSW of PMMA polymer T-joint, International Journal of Advanced Manufacturing Technology, Jul. 2018; 97(1–4): 1445–1456, https://doi.org/10.1007/s00170-018-1847-7
3. Derazkola H. A. and Simchi A., An investigation on the dissimilar friction stir welding of T-joints between AA5754 aluminum alloy and poly(methyl methacrylate), Thin-Walled Structures, Feb. 2019; 135: 376–384, https://doi.org/10.1016/j.tws.2018.11.027
4. Derazkola H. A., Kashiry Fard R., and Khodabakhshi, F. Effects of processing parameters on the characteristics of dissimilar friction-stir-welded joints between AA5058 aluminum alloy and PMMA polymer, Welding in the World, Jan. 2018; 62(1): 117–130, https://doi.org/10.1007/s40194-017-0517-y
5. Haryadi, G. D., Taufik, M., Rochadian, O., Caesarendra, W. and Żak, K. Evaluation of friction stir welding on the microstructure and mechanical properties of dissimilar aluminum alloys 5083-O and 6061-T6 for automotive applications, Advances in Science and Technology Research Journal, 2025; 19(9): 34–49, https://doi.org/10.12913/22998624/205675
6. Aghajani Derazkola, H. and Simchi, A. A new procedure for the fabrication of dissimilar joints through injection of colloidal nanoparticles during friction stir processing: Proof concept for AA6062/PMMA joints, J. Manuf. Process., Jan. 2020; 49: 335–343, https://doi.org/10.1016/j.jmapro.2019.12.008
7. Dalwadi, C. G., Patel, A. R., Kapopara, J. M., Kotadiya, D. J., Patel, N. D. and Rana, H. G. Examination of mechanical properties for dissimilar friction stir welded joint of Al alloy (AA-6061) to PMMA (Acrylic), Mater. Today Proc., 2018; 5: 4761–4765, www.materialstoday.com/proceedings
8. Nagarajan, B. M. and Manoharan, M. Influence of cooling conditions on tensile lap shear strength and microstructure of friction stir welded aluminum alloy 5052-H32 and polycarbonate light weight hybrid joint, J. Manuf. Process., Oct. 2022; 82: 390–402, https://doi.org/10.1016/j.jmapro.2022.08.008
9. Manjunatha C. et al., Experimental investigation and optimization of friction stir welding parameters to manufacture AA6061-B4C composite material using design of experiments, Journal of Materials Science: Materials in Engineering, Dec. 2025; 20(1), https://doi.org/10.1186/s40712-025-00328-2
10. Tucci, F., Carlone, P., Silvestri, A. T., Parmar, H. and Astarita, A. Dissimilar friction stir lap welding of AA2198-AA6082: Process analysis and joint characterization, CIRP J. Manuf. Sci. Technol., Nov. 2021; 35: 753–764, https://doi.org/10.1016/j.cirpj.2021.09.007
11. Sahranavard, M. and Khoramishad, H. Effects of welding parameters and thermal insulation on the mechanical behavior and microstructure of friction lap-welded aluminum to glass fiber–reinforced thermoset composite with a thermoplastic PA6 interlayer, International Journal of Advanced Manufacturing Technology, May 2024; 132(1–2): 727–743, https://doi.org/10.1007/s00170-024-13413-1
12. Pereira, M. A. R., Galvão, I., Costa, J. D. M., Amaro, A. M. and Leal, R. M. Production of aluminium-polymer joints by friction stir spot welding, Journal of Manufacturing and Materials Processing, Aug. 2024; 8(4), https://doi.org/10.3390/jmmp8040179
13. Kasgari, S. A., Aliha, M. R. M., Sadjadi, S. J., Sadowski, T. and Berto, F. Progress in friction stir welding of polymer and aluminum alloys, Mechanics of Composite Materials, Jan. 2024; 59(6): 1083–1100, https://doi.org/10.1007/s11029-023-10158-y
14. Sun, Y., Zhang, Y., Wei, X., Long, H., Sun, Y. and Yang, X. Study on the thermal assistance friction stir lap welding of aluminum alloy and CFRTP, Polym. Compos., Aug. 2024; 45(11): 9899–9910, https://doi.org/10.1002/pc.28446
15. Derazkola, H. A. and Khodabakhshi, F. A novel fed friction-stir (FFS) technology for nanocomposite joining, Science and Technology of Welding and Joining, Feb. 2020; 25(2): 89–100, https://doi.org/10.1080/13621718.2019.1631534
16. Nagarajan, B. M. and Manoharan, M. Enhancement of joint strength of dissimilar aluminum/polymer hybrid joints by friction stir spot welding by surface textures, J. Adhes. Sci. Technol., 2024; 38(8): 1284–1311, https://doi.org/10.1080/01694243.2023.2256557
17. Wang, W., Wang, S., Zhang, X., Xu, Y., Tian, Y. and Huang, H. Enhanced aluminum alloy-polymer friction stir welding joints by introducing micro-textures, Mater. Lett., Jul. 2021; 295, https://doi.org/10.1016/j.matlet.2021.129872
18. Bulto D. and Sinha, D. K. Investigation of physico-mechanical and metallurgical characteristics in a single lap joining of polybutylene terephthalate (PBT) with aluminum alloy through surface modifications, Journal of Engineering and Applied Science, Dec. 2025; 72(1), https://doi.org/10.1186/s44147-025-00686-w
19. Jiang C. Y. et al., Bonding mechanisms of carbon fiber-reinforced plastic/aluminum alloy interface

during friction lap welding via silane coupling treatment, Journal of Materials Research and Technology, Mar. 2024; 29: 3340–3354, https://doi.org/10.1016/j.jmrt.2024.02.026
20. Correia, A. N., Santos, P. A. M., Braga, D. F. O., Baptista, R. and Infante, V. Effects of friction stir welding process control and tool penetration on mechanical strength and morphology of dissimilar aluminum-to-polymer joints, Journal of Manufacturing and Materials Processing, Jun. 2023; 7(3), https://doi.org/10.3390/jmmp7030106
21. Correia, A. N., Braga, D. F. O., Baptista, R. and Infante, V. Tensile and flexural behavior of metal–polymer friction stir buttstrap composite panels, Polymers (Basel)., Aug. 2025; 17(15), https://doi.org/10.3390/polym17152084
22. Nagarajan, B. M. and Manoharan, M. Influence of cooling conditions on tensile lap shear strength and microstructure of friction stir welded aluminum alloy 5052-H32 and polycarbonate light weight hybrid joint, J. Manuf. Process., Oct. 2022; 82: 390–402, https://doi.org/10.1016/j.jmapro.2022.08.008
23. Gagliardi, F., Conte, R., Pulice, D. and Ambrogio, G. Joining feasibility between metallic- And polymeric-based materials by friction stir forming, in Procedia Manufacturing, Elsevier B.V., 2020; 389–394. https://doi.org/10.1016/j.promfg.2020.04.309
24. Yuan, Z., Sun, Y., Long, H.. Zhu, J., Zou, L. and Yang, X. Study on the microstructure and mechanical properties on Al/carbon fiber reinforced thermoplastic dissimilar friction stir lap welding joints, J. Mater. Eng. Perform., Mar. 2024, https://doi.org/10.1007/s11665-024-09482-8
25. Sheikh-Ahmad, J., Zitoune, R., Morel, C., Ferrero, J. F. and Vieille, B. Joining of AA5052 to CF/PEEK by friction lap welding, International Journal of Advanced Manufacturing Technology, May 2024; 132(3–4): 1137–1150, https://doi.org/10.1007/s00170-024-13457-3
26. Khadka, P., Varglund, S., Akinwamide, S. and Vilaça, P. Characterization of friction stir-based linear continuous joining of aluminium alloy to structural polymer, Welding in the World, Jan. 2024; 68(1): 71–90, https://doi.org/10.1007/s40194-023-01622-3
27. MirHashemi, S. M., Amadeh, A. and Khodabakhshi, F. Effects of SiC nanoparticles on the dissimilar friction stir weldability of low-density polyethylene (LDPE) and AA7075 aluminum alloy, Journal of Materials Research and Technology, Jul. 2021; 13: 449–462, https://doi.org/10.1016/j.jmrt.2021.04.094
28. Barakat, A. A., Darras, B. M., Nazzal, M. A. and Ahmed, A. A. A Comprehensive technical review of the friction stir welding of metal-to-polymer hybrid structures, Jan. 01, 2023, MDPI. https://doi.org/10.3390/polym15010220
29. Rudrapati, R. Effects of welding process conditions on friction stir welding of polymer composites: A review, Aug. 01, 2022, Elsevier B.V. https://doi.org/10.1016/j.jcomc.2022.100269
30. Derazkola, H. A. and Khodabakhshi, F. Development of fed friction-stir (FFS) process for dissimilar nanocomposite welding between AA2024 aluminum alloy and polycarbonate (PC), J. Manuf. Process., Jun. 2020; 54: 262–273, https://doi.org/10.1016/j.jmapro.2020.03.020
31. Shinde, G. and Arakerimath, R. Experimental investigation on impact energy of friction stir welded aluminum and copper dissimilar joint using full factorial method, Metallurgical and Materials Engineering, Jun. 2022; 28(2): 335–349, https://doi.org/10.30544/738
32. Das, D., Bag, S., Pal, S. and Sharma, A. Material defects in friction stir welding through thermo–mechanical simulation: dissimilar materials with tool wear consideration, Materials, Jan. 2023; 16(1), https://doi.org/10.3390/ma16010301
33. Melaku, L. E. and Tomków, J. Dissimilar friction stir welding of aluminum to polymer: A review, Sep. 01, 2025, Springer Science and Business Media Deutschland GmbH. https://doi.org/10.1007/s00170-025-16393-y
34. Barakat, A. A., Darras, B. M., Nazzal, M. A. and Ahmed, A. A. A comprehensive technical review of the friction stir welding of metal-to-polymer hybrid structures, Jan. 01, 2023, MDPI. https://doi.org/10.3390/polym15010220
35. Abd Elnabi, M. M., El Mokadem, A. and Osman, T. Optimization of process parameters for friction stir welding of dissimilar aluminum alloys using different Taguchi arrays, International Journal of Advanced Manufacturing Technology, Jul. 2022; 121(5–6): 3935–3964, https://doi.org/10.1007/s00170-022-09531-3